Nanoparticles in dilute gases: Fundamental equivalence between momentum accommodation and surface adsorption

Changran Liu and Hai Wang

Phys. Rev. E **99**, 042127 — Published 19 April 2019

DOI: 10.1103/PhysRevE.99.042127

Nanoparticles in Dilute Gases: Fundamental Equivalence Between Momentum Accommodation and Surface Adsorption

Changran Liu, Hai Wang

Mechanical Engineering Department
Stanford University, Stanford 94305, USA

Abstract

Momentum accommodation is a key factor governing the transport of particles in gases from electric mobility, Brownian diffusion to thermophoresis. This paper explores the relationship between momentum accommodation of nanoparticles in dilute gases and surface adsorption. We demonstrate that the momentum accommodation factor is fundamentally equal to the probability of surface adsorption. Molecular dynamic simulations show that surface adsorption is the key mechanism behind the diffuse scattering model; and that upon gas-particle collision the immediate reflection dynamics and surface adsorption events are governed by the kinetic energy distribution of the rebounding gas molecules. This distribution determines the transition of the dominant mode of molecular scattering off a particle surface from diffuse to specular elastic reflection as the particle approaches the realm of molecular size. The kinetics and equilibrium of physisorption are examined to shed light on the effect of the lifetime of surface adsorbates on momentum transfer. A statistical treatment is proposed for the adsorption and hence the gas-nanoparticle momentum accommodation coefficient. The validity of the theoretical treatment is examined by comparing its prediction against experimental mobility data of silver nanoparticles.

Submitted to

Physical Review E

January 2019

Revised March 2019

I. INTRODUCTION

A basic understanding of momentum accommodation of particles in dilute gases is critical to studies of a wide range of transport and reaction processes in aerosols and large molecules in gases [1-8]. In reactive aerosol flows ranging from soot or other nanoparticle formation in flames [9-12], catalysis of freely suspended nanoparticles [13,14] to heterogeneous and homogeneous nucleation and growth [15-17], the adsorption and desorption of gas molecules and the subsequent gas-surface reactions are often tightly coupled with the particle transport process. A key historic account of the particle transport problem dates back to Millikan's experiments on oil drops in an electric field [18] and Epstein's gas-kinetic analysis of the drag force on particles with the rigid-body assumption [19]. The momentum accommodation factor φ was borne out of the oil-drop data interpretation and analysis. Millikan [20,21] found that in the large Knudsen number regime his data could be explained satisfactorily by a mix of 90% diffuse scattering and 10% specular scattering as the average outcome of gas-particle collisions, or equivalently by a linear combination of Epstein's drag forces in the diffuse and specular elastic scattering limits,

$$F = \varphi F_d + \left(1-\varphi\right) F_s, \tag{1}$$

with φ = 0.9. For a particle with radius R at the drift velocity V, Epstein gave the following drag force expressions in the specular and diffuse scattering limits, respectively:

$$F_s = \frac{8}{3}\sqrt{2\pi m_g k_B T}\, NR^2 V \ , \tag{2}$$

and

$$F_d = \frac{8+\pi}{3}\sqrt{2\pi m_g k_B T}\, NR^2 V \ . \tag{3}$$

where k_B is the Boltzmann constant, m_g, N and T are the mass, number density and temperature of the gas, respectively. Suffice it to note that Millikan conducted his experiments in air at room temperature. The smallest drop tested has a radius of 20 nm. There is little to no evidence that a constant φ and the 0.9 value is applicable to smaller particles and for other gases under other thermodynamic conditions.

By contrasting the available molecular transport theory with Millikan's oil drop transport, it can be readily concluded that momentum accommodation cannot be a constant [2,22]. The

Chapman-Enskog theory [23] treats molecular collisions to be specular elastic (φ = 0). It successfully explained many molecular transport properties including the binary diffusion coefficient of small molecules in dilute gases. Taking Millikan/Epstein's result on oil drops and the Chapman-Enskog theory together, we find that a general treatment of the momentum accommodation requires a consideration of its variation with respect to the particle size to the realm of molecular sizes. Analysis of the available electric mobility data of nanoparticles of four different particle materials in air at room temperature suggests that the momentum accommodation factor does decrease from a value of 0.9 to 0 as the particle size decreases; the transition takes places at a particle size of several nanometers and is quite abruptly with respect to the particle size [22,24]. Currently, a theoretical treatment for the aforementioned transition of gas-particle momentum accommodation is unavailable.

Earlier, a molecular dynamics (MD) study [25] offered a qualitative, molecular-level explanation for the two collision models of Epstein. In that study, two distinctive outcomes of gas-particle collisions were revealed. They differ in the degree of gas-particle momentum accommodation. The first outcome is immediate reflection—a specular-like process. Although the reflections are almost never exactly elastic due to stochasticity of the collision process, the momentum transfer is found to be specular elastic on average. The second outcome is gas adsorption on the particle surface. Adsorption leads to diffuse scattering [24,25] because the ensuing surface random walk of the adsorbed molecule and its eventual desorption retains little to no memory about its incident momentum or even the initial point of contact. The desorbing gas molecule behaves as if it undergoes diffuse scattering.

The purpose of the current work is to take the work just discussed a step further. We demonstrate the momentum accommodation factor and surface adsorption probability are fundamentally equivalent. For this purpose, we carry out MD simulations to demonstrate this equivalence. Specifically, the kinetic energy distribution of gas molecules during their rebound is studied as a function of temperature, gas density, particle size, and surface coverage. A statistical theory is then proposed for the probability of gas adsorption on particle surfaces employing the MD data in the treatment. Simulations are carried out for two systems: the collisions of

buckminsterfullerene (C_{60}) with argon and of a silver nanoparticle with nitrogen (N_2) and in a bath of N_2. The C_{60}-Ar system provides physical insights into the problem. Silver nanoparticle was chosen because mobility data are available in the size range in which the specular-to-diffuse scattering transition has been observed [24]. The MD results are also used to enable a comparison of the theoretical momentum accommodation factor against experimental data. To examine the implication of the finite lifetime of surface adsorbates in momentum transfer, our MD simulations also extend to a study of the kinetics of physisorption and desorption and their equilibrium.

II. SIMULATION METHOD

GROMACS and leap-frog integration scheme [26] were used for the Ar-C_{60} simulation in a microcanonical ensemble (60C+1Ar, E) in which a single Ar atom with a given incident velocity is sent toward the C_{60}. The Ar-C atom pairwise interactions are computed using the Lennard-Jones 12–6 potential function,

$$\Phi(r) = 4\varepsilon \left[(\sigma/r)^{12} - (\sigma/r)^{6}\right], \tag{4}$$

where r is the separation distance. The collision diameter σ and potential well-depth ε for Ar and C atoms are estimated using the empirical mixing rule with $\sigma = (\sigma_g + \sigma_p)/2$ and $\varepsilon = (\varepsilon_g \varepsilon_p)^{1/2}$, where $\sigma_g = \sigma_{\mathrm{Ar}} = 3.4$ Å, $\varepsilon_g/k_B = \varepsilon_{\mathrm{Ar}}/k_B = 120$ K, $\sigma_p = \sigma_{\mathrm{C}} = 3.47$ Å, $\varepsilon_p/k_B = \varepsilon_{\mathrm{C}}/k_B = 33.3$ K [27]. The total potential energy between Ar and C_{60} is calculated as the sum of the Ar-C pairwise potentials. An increase in ε effectively deepens the gas-particle potential well. Higher-order, three body interactions are neglected. The intramolecular potential of C_{60} was taken from [28]. The C_{60} molecule is initialized with the atom-velocity variance in accordance with the Boltzmann distribution at a prevailing temperature. After relaxation for 10 ps, collision is initiated by sending a single Ar atom 2 nm away from the particle surface towards the center of C_{60} at a given incident speed. Another 10 ps simulation follows to explore the collision features.

MD simulations were performed also for an Ag particle with nitrogen (N_2) in both microcanonical and canonical ensembles. In the microcanonical ensemble, the simulations aimed to resolve the effect of N_2 rotation on the absorption probability, as discussed in [29] A bulk of the simulations was conducted in the canonical ensemble, in which gas-particle physisorption kinetics and equilibrium, the distribution of the post-collision kinetic energy and its relationship to the surface adsorption probability were studied in detail. The N_2-Ag atom pairwise interactions were computed using Eq. (4). The self-collision potential parameters adopted here are: σ_{N_2} = 3.652 Å, ε_{N_2}/k_B = 98.4 K [30], and σ_{Ag} = 2.54 Å, ε_{Ag}/k_B = 3995.5 K [30]. Silver particles were constructed from a face centered cubic (FCC) crystal by removing atoms that lie outside a certain radius. The numbers of the Ag atom are 28, 101, 242, 826 and 1976 for particle radius R = 0.5, 0.75, 1.0, 1.5, and 2.0 nm, respectively. The tight binding potential function [31] was employed for Ag-Ag intra-particle potential. The potential function has been verified against bulk material properties including the mass density and melting point. The equations are solved using Beeman's leapfrog algorithm [32], with time step equal to 1 fs. In each simulation, a single Ag particle with a bare surface is initialized in a N_2 bath of over 863 N_2 molecules. The initial velocities of the N_2 molecules and silver atoms were assigned with a pre-specified temperature. At 300 K and 1 atm, the physical dimension of the MD system is 32.8^3 nm^3. Since the largest particle size simulated is R = 2 nm, the computational domain is large enough to allow for the use of period boundary condition. The N_2 rotational and vibrational effects are neglected. The system temperature is re-scaled periodically (every 50 ps) such that the system maintains the target temperature in spite of the minor temperature rises due to exothermic gas adsorption.

III. RESULTS

A. The Ar-C_{60} system

Two collision outcomes, immediate reflection and surface adsorption, are illustrated in Fig. 1(a) using the Ar-C_{60} system as the example. The distinctive outcomes are primarily related to the kinetic energy of the gas immediately following the collision (E'). For the gas to escape the attractive force field, E' must be larger than a certain threshold E_{esc} above which the force is insufficient to attract Ar back to the particle surface. E' is a function of the distance between the gas molecule and particle because of the interplay between potential and kinetic energies. For convenience, we evaluate E' at a critical rebound radius r^* which is defined as the distance of the reflected gas to the mass center of the particle above which the variation in the potential energy practically vanishes. All rebound trajectories must still reach the critical radius, including those that would lead to gas adsorption eventually. The thus-defined E' is a stochastic quantity in part due to molecular vibration in the particle. For the Ar-C_{60} pair, the critical r^* may be chosen to be 10.5 Å for an incident gas velocity of 72.5 m/s, an initial C_{60} vibrational temperature of 50 K and the impact factor b = 0. The choice for the r^* value is not unique, but choosing a different r^* merely shifts the mean E' value; it would not affect the subsequent analysis.

A sample distribution of E' is evaluated from 400 MD trajectories and presented in Fig. 1(c). The immediate reflection and adsorption events are marked by the different grey intensities or colors in the histogram. Several observations can be made from Fig. 1(c). First, the distribution may be modeled by the Gamma distribution,

$$P_{E'}\left(E'\right)=\frac{D^{-1/c^2}}{\Gamma\left(1/c^2\right)}E'^{\left(1/c^2-1\right)}\exp\left(-\frac{E'}{D}\right), \tag{5}$$

where Γ() is the Gamma function, $c=\sigma_{E'}/\overline{E}'$ is the coefficient of variation of E', $D = c\sigma_{E'}$ is the index of dispersion, $\overline{E}'$ is the mean post-collision energy, and $\sigma_{E'}^2$ is the variance. Clearly, $\overline{E}'$ and $\sigma_{E'}$ are functions of the incident kinetic energy of the gas and particle temperature. The Gamma distribution was chosen for convenience because of its attractive mathematical properties and the fact that it is one of the most versatile two-parameter distributions. The interactions of the gas molecule with the particle are localized and involve mostly several surface

atoms at a time. For this reason, $\bar{E}'$ and $\sigma_{E'}$ are weak functions of the impact parameter and particle size.

The transition from immediate reflection to surface adsorption is rather abrupt with respect to E' as shown in Fig. 1(c). For this reason, the probability of adsorption $P_a(E')$ can be modeled by a step function

$$P_a\left(E'\right)=\begin{cases} 1 & \text{for } E' \le E_{esc} \\ 0 & \text{for } E' > E_{esc} \end{cases} \tag{6}$$

where the escape energy E_{esc} is defined as the kinetic energy of at which exactly ½ the gas molecules is attracted back to the particle surface undergoing adsorption.

The probability of surface adsorption may then be defined as

$$\pi = \int_0^{\infty} P_a\left(E'\right) P_{E'}\left(E'\right) dE' . \tag{7}$$

Putting eqs (5) and (6) into eq (7), we find

$$\pi = \int_0^{E_{esc}} \frac{D^{-1/c^2}}{\Gamma\left(1/c^2\right)} E'^{\left(1/c^2-1\right)} \exp\left(-\frac{E'}{D}\right)\, dE' . \tag{8}$$

The parameters needed to evaluated the above equation are E_{esc}, $\bar{E}'$ and $\sigma_{E'}$, and they may be evaluated from the E' distribution. Compared to the probability of surface adsorption directly calculated from the MD simulations, Eq. (8) produces the MD results rather well as it can be seen in Fig. 1(d). For the comparison, we varied the self-collision well depth of the gas ε_g to mimic the change of the well depth between the gas molecule and C_{60}. Clearly, the adsorption probability increases with an increase in the gas-particle binding energy.

For the system considered all adsorbed gas molecules would desorb at some point. If the adsorbate lifetime is long enough, the overall process of adsorption-surface random walk-desorption has the same effect as diffuse scattering as far as the gas-particle momentum transfer is concerned. From this consideration, an adsorbing event is equivalent to diffuse scattering for which the momentum of the gas is fully accommodated; and a non-adsorbing event is specular-elastic like for which the momentum accommodation is zero. It follows that the probability of surface adsorption and momentum accommodation coefficient are completely equivalent.

B. Kinetics and Equilibrium of Physisorption

Kinetics and equilibrium of physisorption can play a role in the gas-particle momentum accommodation in several ways. The time evolution from a bare particle surface to a surface undergoing equilibrium adsorption and desorption could produce certain transient effects in momentum transfer if the kinetic process is slow relative to the time scale of particle transport. At adsorption/desorption equilibrium and depending on the surface coverage, the surface adsorbates can interact with incident gas, thus leading to secondary collision events that involve one or more adsorbates. Again depending on the surface coverage and particle size, the adsorbates cause the particle to be larger and hence, a potentially larger momentum accommodation coefficient than when the particle is bare.

The kinetics and equilibrium of physisorption of N_2 on Ag particle was simulated in the canonical ensemble for 1.6 ns. In the simulation, N_2 rotation is neglected. The effect is shown to be unimportant for the current problem, as discussed in [29]. A bare Ag particle was introduced into an N_2 bath gas at a prescribed pressure. The vibrational temperature of the particle was set to be equal to the gas temperature. Typical MD time profiles of the number of adsorbates per particle are presented in Fig. 2 for three particle sizes (top panel) and for R = 1 nm under several thermodynamic conditions. Over the range of conditions calculated, the time to reach adsorption and desorption equilibrium is rapid, <O(1 ns), indicating that the relaxation to equilibrium poses no influence on momentum accommodation in typical reactive flows.

The net rate of adsorption can be described by the competition between adsorption or the influx to the particle surface and desorption or outflux from the particle surface:

$$\frac{dn}{dt} = I - \frac{n}{\overline{\tau}}\ , \tag{9}$$

where n is the number of N_2 molecules adsorbed, I is the rate of adsorption on the particle, and $\overline{\tau}$ is the mean lifetime of the adsorbate. Integration of eq. (9) yields

$$n = I\overline{\tau}\left(1 - e^{-t/\overline{\tau}}\right). \tag{10}$$

In principle, I may be evaluated from the wall collision rate, but since for a particle just a few nanometers in size its surface area can be difficult to define, I is treated here as a fitting parameter. Along with $\overline{\tau}$, the MD results are fitted to Eq. (10), as shown by the dashed lines of Fig. 2. The mean lifetime of the adsorbate is plotted in Fig. 3 as a function of temperature for a particle with R = 1 nm. It can be seen that $\overline{\tau}$ is of the order of 0.1 ns, and it decreases with an increase in temperature. The velocity of random walk of the adsorbates on the particle surface may be estimated from the root mean squared velocity of N_2 on a 2-D surface and the energy barrier for surface hopping. If the hopping energy barrier is 1 kcal/mol, the $\overline{\tau}$ values of Fig. 2 gives a minimum length of O(10 nm) for the surface random walk of the adsorbates, which is large compared to the particle size. Furthermore, the inset of Fig. 3 shows the distribution of τ at 300 K. Around 25% of the adsorbed N_2 have a lifetime < 33 ps, corresponding to a random-walk length of ~2 nm, which is still long compared to the particle size. The lifetime distribution follows an exponential decay function, which is consistent with a fully de-correlated statistical process: mathematically the exponential distribution is one of the only two distributions that are associated with memoryless events [33]. This and the surface random walk length argument indicate that the desorbed N_2 should retain no memory of its incidence under the conditions tested. Yet the adsorbate lifetime is short enough so that surface adsorption followed by desorption effectively governs the gas-particle momentum transfer mechanism with the net effect identical to that of the diffuse scattering, or one of the two reflection models assumed in the gas-kinetic theory analyses of Epstein [19] and Li and Wang [2].

With the presence of adsorbates, gas-particle collisions can have two additional outcomes, both of which stem from gas collision with a surface adsorbate, instead of the particle material. The first outcome involves the exchange of the incident gas with an adsorbate, which is specular like on average. The second outcome involves the rebound of the gas molecule upon its collision with the adsorbate. The surface adsorbate usually dampens the force of interaction between the rebounding gas molecule and particle surface atoms. Therefore, both outcomes lead to a reduced probability of adsorption. On the other hand, an enlarged particle size due to adsorption increases

the collision cross section and an increased probability of adsorption. The two effects compensate each other, and the net impact on momentum accommodation coefficient is expected to be small. For the cases studied here, the maximum surface coverage was found to be around 30%. The coverage is determined by dividing the number of adsorbed molecules by the number of particle surface atoms. Hence, the probability of striking into a surface adsorbate is significant, but not dominating compared to direct N_2-Ag interactions.

An even more interesting aspect of the problem is that since physisorption is also a necessary first step to gas-surface reactions, the analysis here offers a unique point of view about a unified treatment for nanoparticle transport and reaction in gases. In nanoparticle catalysis, the surface coverage of reactant(s) plays a major role in the reaction rate. Evidence concerning the size dependency of catalytic activity is abundant (see, e.g., [34-36]). Empirically, a critical particle size has been observed below which the catalytic activity diminishes [34]. In nucleation and surface growth, the Kelvin effect provides a thermodynamic explanation for vapor condensation on available particle surface through a consideration of the critical particle radius and surface tension [37]. The understanding garnered here offers a coherent view involving momentum transfer and accommodation and the kinetic and equilibrium processes of gas-particle processes.

C. Probability of Surface Adsorption

As discussed in Section III.A and also shown in Fig S1 of [29], the outcome of a collision is determined by the competition between the post-collision kinetic energy of the gas and the gas-particle attractive force during the initial gas rebound. For all other things being equal, a larger particle gives a higher surface adsorption probability because of the increased potential energy of interaction during gas rebound following the initial contact; and a higher gas incident velocity leads to a reduced surface adsorption probability, because of a correspondingly higher rebound kinetic energy. The immediate reflection events are those with the gas molecules having enough kinetic energy to overcome the attractive force, thus escaping the gas-particle potential field.

To illustrate the above point, post-collision kinetic energy distributions were evaluated at $r^* = R + 0.5$ nm from simulations of a single Ag particle in a N_2 bath after the system reached the absorption/desorption equilibrium. The results are plotted in Fig. 4 over a range of particle size at $T = 300$ K. In these plots, E' is normalized as $\mu = E'/\sigma_{E'}$. Over 100 collision events were considered for each E' bin. Also included in the plots are the Gamma distribution fits to the MD data (Eq. 5). In general, the histograms are "noisier" than that of the Ar-C_{60} system in which the variations of the initial condition are substantially smaller. Here, the greater levels of "noises" are obviously due to the variations of the gas kinetic energy, the impact factor, and for smaller particles, their more irregular surfaces. The magnitude of energy fluctuation in the particle increases with an increase in its temperature. Nevertheless, the Gamma distribution still works well, as evidenced by the results shown in Fig. 4 and also the series of histograms for a fixed particle radius ($R = 1$ nm), but at several temperatures, as shown in Fig. 5. Also shown are the E' distributions for collision events that lead to immediate reflection (the shaded bars) and the distributions corresponding to adsorption (the open bars). Qualitatively, the MD results discussed thus far are consistent with the statistical treatment proposed in Section III.A.

The probability of surface adsorption can be treated by Eq. (8) with E_{esc}, $\bar{E}'$ and $\sigma_{E'}$ as the input parameters. As discussed in section III.A, these parameters may be evaluated from MD simulations. Here we simplify Eq. (8) by nondimensionalizing it,

$$\pi = \frac{1}{\Gamma\left(1/c^2\right)} \int_0^{\mu_{esc}} \frac{\mu^{\left(1/c^2-1\right)}}{c^{1/c^2}} \exp\left(-\mu/c\right) d\mu, \tag{11}$$

where the dimensionless post-collision kinetic energy μ is defined as

$$\mu = E'/\sigma_{E'} = E'/c\bar{E}', \tag{12}$$

and the dimensionless escape energy μ_{esc} is

$$\mu_{esc} = \bar{E}_{esc}/c\bar{E}', \tag{13}$$

The notation $\overline{E}_{esc}$ is used for a system in which the particles immersed in a bath gas so as to distinguish it from E_{esc} used in the earlier case of single gas-particle pair interactions. Furthermore, we consider the energy conservation of a collision event,

$$E' = E_i - \Phi\left(r^*\right) - \Delta E, \tag{14}$$

where $\Phi\left(r^*\right)$ and ΔE are the potential energy and kinetic energy exchange during collision, respectively. ΔE is taken to be positive if the gas loses energy to the particle, and negative if the gas gains energy. Averaging E_i over the Boltzmann energy distribution, we find

$$\overline{E}' = \overline{E}_i - \Phi\left(r^*\right) - \overline{\Delta E}, \tag{15}$$

where $\overline{\Delta E}$ is the average of ΔE over the incident kinetic energy distribution. $\overline{\Delta E}$ increases with an increase in the difference of the gas incident kinetic energy and the mean vibrational energy of the particle $\overline{E}_s$ [38,39]. As a first approximation, we let $\overline{\Delta E} = \lambda\left\{\left[\overline{E}_i - \Phi\left(r^*\right)\right] - \overline{E}_s\right\}$, where λ ($0 \le \lambda \le 1$) may be interpreted as the energy accommodation factor. If the gas and particle are equilibrated, we have $\overline{E}_i = \overline{E}_s$ and

$$\overline{E}' = \overline{E}_i - \left(1-\lambda\right)\Phi\left(r^*\right). \tag{16}$$

The above treatment yields three dimensionless parameters (μ_{esc}, λ and c) for evaluating Eq. (11).

To simplify the treatment further, we note that the escape energy μ_{esc} is determined largely by the attractive gas-particle force and is therefore related to the potential energy at r^*. To illustrate this point, we plot μ_{esc} in Fig. 6 as a function of the dimensionless potential energy $\Phi(r^*)/c\bar{E}'$, varying particle size, temperature, and gas density. Here, the potential function of Rudyak et al. [40] is adopted to evaluate $\Phi(r^*)$,

$$\Phi\left(r\right) = \Phi_9\left(r\right) - \Phi_3\left(r\right), \tag{17}$$

where

$$\Phi_i(r) = C_i\left\{\left[(r-R)^{-i} - (r+R)^{-i}\right] - a_i\left[(r-R)^{-i+1} - (r+R)^{-i+1}\right]\right\},$$

$$a_9 = 9/(8r)$$

$$a_3 = 3/(2r),$$

$$C_9 = 4\pi\varepsilon\sigma^{12}/(45V).$$

$$C_3 = 2\pi\varepsilon\sigma^{6}/(3V).$$

In the above equations, $V = \bar{M}/\rho_s$, where ρ_s and $\bar{M}$ are the mass density and mean atomic mass of the particle material. The parameters σ and ε are gas-particle atom pairwise potential parameters identical to those employed in the current MD simulation (see, section II).

Over the particle size range considered, μ_{esc} is seen to vary linearly with $\Phi(r^*)/c\bar{E}'$:

$$\mu_{esc} \cong -1.45(\times/\div 1.1)\Phi(r^*)/c\bar{E}'. \tag{18}$$

To examine how general the relationship is, we also plot in Fig. 6 the μ_{esc} values varying T (150 and 450 K) and gas density N at $0.5N_0$ and $2N_0$, where N_0 is the density at p = 1 atm. Clearly, the influence of temperature and gas density is rather weak on the relationship, and as such the dashed lines bracket the uncertainty in the proportionality. The uncertainty factor is found to be 1.1 as given in Eq. (18). With the above treatment, only two parameters are now needed to evaluate Eq. (11). They are the energy accommodation factor λ and the coefficient of variation c.

The λ values were evaluated from MD simulations over ranges of particle size, temperature, and gas density. They are listed in Table 1. Over the ranges tested, λ is basically a constant and equal to 0.80 with a standard deviation of 0.02. The coefficient of dispersion c also shows small variations. Its average value is 0.49 and the standard deviation is 0.04. The last three columns of Table 1 compare the adsorption probabilities calculated directly from MD and from Eq. (11) using the μ_{esc}, λ and c values individually evaluated by MD, and from the same equation but using μ_{esc} of Eq. (18) and the mean λ and c values listed on the bottom row of Table 1. The comparisons are also provided in Fig. 7. Clearly, the simplifications discussed above reproduce the MD results well. Sensitivity of π to λ and c is negligible as shown in Fig. 8, but the sensitivity

to μ_{esc} can be appreciable. Yet in all cases, the variation for π is smaller than the scatters in available data, as will be discussed below.

D. Quantitative Equivalence between Adsorption Probability and Momentum Accommodation Factor

We demonstrate here the quantitative equivalence between the probability of surface adsorption π and the momentum accommodation coefficient φ by comparing the prediction of Eq. 11 with available mobility data of silver nanoparticles in N_2 (or air). To start, we discuss first the 0.9 value commonly assumed for the momentum accommodation factor. We used the Ag particle in N_2 as the example and calculated π or equivalently φ as a function of R at several temperatures all under 1 atm pressure. The results are shown in Fig. 9. As is seen, φ is not a constant. It increases with an increase in the particle size. At 300 K, the transition from immediate reflection with $\varphi = 0$ to absorbing collision (φ approaches unity) occurs at a few nanometers in particle radius. Importantly, we find φ approaches 0.8 as R grows to 10 nm, which is close to the emprical φ value of 0.9 from Millikan oil-drop data ($R > 20$ nm). Of course, there is no theoretical reason why φ should be 0.9 under all conditions. Fig. 9 demonstrates that the limiting φ values is dependent on temperature. At 150 K and for large particles, φ exceeds 0.9; and the specular-to-diffuse transition is sharper with respect to the particle size and occurs at a smaller size than at 300 K. Conversely, at 450 K, φ asymptotes to a value smaller than 0.9 and the transition is slower with respect to the particle size. The above result illustrates the fact that the momentum accommodation factor should never be considered as a constant, and that the 0.9 value widely adopted in aerosol and other studies is applicable only for room temperature and oil droplet in air, nitrogen or air-like bath gases.

Among the available mobility data of silver nanoparticles, Kuga et al. [41] and Scheibel et al. [42] determined the particle size by transmission electron microscopy; de la Mora and coworkers [43] measured particle mass by aerodynamic impaction. The reported mobility data may be recast into the corresponding values of the reduced collision integral for each particle size [24]:

$$\Omega^{(1,1)*} = \frac{3q}{8\sqrt{2\pi m_r k_B T}\, NR^2} \frac{1}{Z}, \tag{19}$$

where q and Z are the particle charge and measured mobility, respectively, and m_r is the reduced mass. The $\Omega^{(1,1)*}$ values derived from the experimental mobility data are shown in Fig. 10 as a function of the particle radius by the open symbols.

Equation (19) was derived from a gas-kinetic theory analysis of drag on particle for Kn >> 1 [2,43], given as

$$F_{d/s} = \left(8/3\right)\sqrt{2\pi m_r k_B T}\, NR^2 \Omega_{d/s}^{(1,1)*} V \tag{20}$$

where F_d and F_s are the drag forces for specular and diffuse scattering, respectively. We have demonstrated previously that Eqs. (2) and (3) are the special cases of Eq. (20) in the rigid body limit [2]. In Eq. (20), $\Omega_d^{(1,1)*}$ and $\Omega_s^{(1,1)*}$ are the respective reduced collision integrals given in [2]. They have been parameterized [22] for the gas-particle potential function of Rudyak et al. [40],

$$\Omega_d^{(1,1)*} = 1 + \frac{\pi}{8} + \left[1.072 + \frac{2.078}{T^{*1/4}} + \frac{1.261}{T^{*1/2}}\right]\sigma' + \left[3.285 - \frac{8.872}{T^{*1/4}} + \frac{5.225}{T^{*1/2}}\right]\sigma'^2, \tag{21}$$

and

$$\Omega_s^{(1,1)*} = 1 + \left[0.316 + \frac{1.47}{T^{*1/4}} + \frac{0.476}{T^{*1/2}}\right]\sigma' + \left[1.53 - \frac{5.013}{T^{*1/4}} + \frac{4.025}{T^{*1/2}}\right]\sigma'^2, \tag{22}$$

where $\sigma' = \sigma/R$, $T^* = kT/\varepsilon'$, and $\varepsilon' = 2\pi\varepsilon\sigma^3/3V$. The dashed lines of Fig. 10 are calculated using the above equations with the potential parameter values identical to those used in the current MD simulation. As is seen, the experimentally-derived reduced collision integrals are bracketed by the theoretical collision integrals in the specular and diffuse limits. The comparison highlights the transition of the dominant mode of momentum transfer from specular scattering at a small particle size to diffuse scattering at larger sizes.

de la Mora et al. [43] measured the particle mass for silver particles over a range of particle sizes. To convert mass to particle size, we utilized the MD geometries to determine the material

density through a measure of the average distance of particle mass center to the surface atoms. Method 1 assumes the particle radius to be the sum of the aforementioned distance and σ, while Method 2 use $\sigma_{Ag}/2$ to account for the particle "surface volume". As shown in the inset of Fig. 10, both methods predict a decrease of the mass density as the particle size decreases, as expected. Method 2 yields a mass density that converges to the value of bulk silver. Because the particle mass in de la Mora et al. [43] was derived from aerodynamic impaction and hence the carrier gas adsorption on the particle surface is of importance to the measured particle mass, the density values from Method 1 are adopted. We assume here that the particles are spherical.

For comparison of our statistical treatment with experimental data, we define an effective reduced collision integral in the same manner as Eq. (1), i.e., $\Omega^{(1,1)*} = \varphi\Omega_s^{(1,1)*} + (1-\varphi)\Omega_d^{(1,1)*}$. Equating π and φ, and combining the above equation with Eq. (11), we obtain

$$\Omega^{(1,1)*} = \frac{1}{\Gamma\left(1/c^2\right)}\left\{\Omega_s^{(1,1)*}\int_0^{\mu_{esc}} \frac{\mu^{\left(1/c^2-1\right)}}{c^{1/c^2}}\exp\left(-\frac{\mu}{c}\right)d\mu + \Omega_d^{(1,1)*}\int_{\mu_{esc}}^{\infty} \frac{\mu^{\left(1/c^2-1\right)}}{c^{1/\bar{c}^2}}\exp\left(-\frac{\mu}{c}\right)d\mu\right\}. \qquad (23)$$

The above expression reproduces the experimental data well as shown in Fig. 10. Also shown in the figures are predictions using the φ values by directly following >100 MD collisions for several particle radii (R = 0.5, 1, 1.5 and 2 nm). Clearly, Eq. (23) reproduces the MD results also well.

Fig. 11 presents a similar $\Omega^{(1,1)*}$-versus-R analysis for Cu_2O and polyethylene glycol (PEG) particles. The mobility data of Cu_2O [40] and PEG [44,45] were converted to the reduced collision integrals in a similar manner. The potential parameters of N_2-Cu_2O and N_2-PEG and the collisional integrals for the limiting scattering cases are taken from Ref. [24] again using the potential function of Rudyak et al. [40]. In principle, the data shown can be modeled with MD, but this is beyond the scope of the present work. Here, Eq. (23) was used to fit the data. It was found that λ = 0.8 also works well for both Cu_2O and PEG particles. The coefficient of dispersion c is the only fitting parameter. Its value was found to be 0.04 and 0.24 for Cu_2O and PEG, respectively. As shown in Fig. 11, a smaller coefficient of dispersion produces a sharper

transition in the transition of momentum transfer with respect to R.

The observation about the relationship between particle mobility and surface energy by Jung *et al*. [3] is consistent with the current result. A higher surface energy leads to a great tendency for a particle to adsorb its surrounding gas molecules, and hence a more efficient momentum accommodation. The relationship between particle surface energy and the E' distribution is another fruitful area for further investigation.

IV. CONCLUSION

We performed MD simulations to elucidate the critical role of surface adsorption in gas-particle momentum accommodation. The diffuse scattering is in fact the result of surface adsorption of the gas. The transition from specular scattering at small particle sizes to diffuse scattering toward large size is caused by an increased ability of the particle to accommodate the incident kinetic energy of the gas due to the more significant potential energy of gas-particle interactions. A statistical theory is proposed for the momentum accommodation coefficient based on these observations. The validity of the key assumptions in the statistical theory has been examined by the MD simulations over a range of particle size, temperature and pressure for silver particles in nitrogen (N_2). The kinetic energy distribution of the gas molecules during their rebound is found to be critical to the two collision outcomes, namely specular scattering and diffuse scattering, and this distribution is dependent on gas temperature and density, particle size, and to an extent, surface coverage of the gas adsorbate. Within the framework of the statistical treatment proposed, these dependencies fundamentally impact the probability of surface adsorption and the gas-particle momentum accommodation and their relationships to the gas and particle properties.

Three parameters are required to evaluate the momentum accommodation coefficient using the statistical treatment proposed. These are, the coefficient of dispersion of the kinetic energy distribution of the rebounding gas c, the dimensionless escape energy μ_{esc}, and the energy accommodation coefficient λ, all of which may be determined from MD simulations. Moreover,

MD results show that two of the three parameters (c and λ) may be treated as constants for a given gas-particle system, independent of the thermodynamic condition of the gas and the particle size. The third parameter, i.e., the escape energy μ_{esc}, may be determined from the gas-particle potential function. The statistical treatment just discussed is shown to reproduce available mobility-versus-size data of silver particles in air or nitrogen. Also demonstrated is the application of the theory in fitting available experimental mobility data of Cu_2O and polyethylene glycol over a range of particle sizes.

Suffice it to note that adsorption is the first step in catalytic reaction, nucleation, and particle surface growth. If gas-particle momentum accommodation and physisorption are equivalent, a study of one phenomenon naturally lends to the understanding of the other, and as such the conclusion of the current study offers an opportunity for us to advance a generalized treatment for transport, nucleation and gas-surface physicochemical processes of nanoparticles in gases.

Acknowledgement
The work was support by the US Air Force Office of Scientific Research (AFOSR) under grant number FA9550-16-1-0486.

V. REFFERENCES

[1] J. H. Kim, G. W. Mulholland, S. R. Kukuck, and D. Y. H. Pui, J. Res. Natl Inst. Stan. **110**, 31 (2005).

[2] Z. Li and H. Wang, Phys. Rev. E **68**, 061206 (2003).

[3] H. Jung, K. Han, G. W. Mulholland, D. Y. H. Pui, and J. H. Kim, J. Aerosol Sci. **65**, 42 (2013).

[4] C. J. Hogan Jr, B. T. Ruotolo, C. V. Robinson, and J. Fernández de la Mora, J. Phys. Chem. B **115**, 3614 (2011).

[5] C. Larriba, C. J. Hogan Jr, M. Attoui, R. Borrajo, J. F. Garcia, and J. Fernández de la Mora, Aerosol Sci. Technol. **45**, 453 (2011).

[6] C. Larriba and C. J. Hogan Jr, J. Phys. Chem. A **117**, 3887 (2013).

[7] C. Liu, Z. Li, and H. Wang, Phys. Rev. E **94**, 023102 (2016).

[8] C. Liu, R. Zhao, R. Xu, F. N. Egolfopoulos, and H. Wang, Proc. Combust. Inst. **36**, 1523 (2017).

[9] H. Wang, Proc. Combust. Inst. **33**, 41 (2011).

[10] S. Nikraz, D. J. Phares, and H. Wang, J. Phys. Chem. C **116**, 5342 (2012).

[11] C. Saggese, A. Cuoci, A. Frassoldati, S. Ferrario, J. Camacho, H. Wang, and T. Faravelli, Combust. Flame **167**, 184 (2016).

[12] C. Liu, J. Camacho, and H. Wang, ChemPhysChem **19**, 180 (2018).

[13] T. Shimizu, A. D. Abid, G. Poskrebyshev, H. Wang, J. Nabity, J. Engel, J. Yu, D. Wickham, B. Van Devener, and S. L. Anderson, Combust. Flame **157**, 421 (2010).

[14] B. Van Devener, S. L. Anderson, T. Shimizu, H. Wang, J. Nabity, J. Engel, J. Yu, D. Wickham, and S. Williams, J. Phys. Chem. C **113**, 20632 (2009).

[15] P. Chakraborty and M. R. Zachariah, J. Phys. Chem. A **112**, 966 (2008).

[16] S. Takahama and L. M. Russell, J. Geophys. Res. Atmos. **116** (2011).

[17] W. G. Courtney, J. Chem. Phys. **35**, 2249 (1961).

[18] R. A. Millikan, Philos. Mag. **34**, 1 (1917).

[19] P. S. Epstein, Phys. Rev. **23**, 710 (1924).

[20] R. A. Millikan, Phys. Rev. **21**, 217 (1923).

[21] R. A. Millikan, Phys. Rev. **22**, 1 (1923).

[22] Z. Li and H. Wang, Phys. Rev. E **68**, 061207 (2003).

[23] T. G. Cowling and S. Chapman, *The mathematical theory of non-uniform gases* (University Press, 1960).

[24] H. Wang, Ann. N. Y. Acad. Sci. **1161**, 484 (2009).

[25] Z. Li and H. Wang, Phys. Rev. Lett. **95**, 014502 (2005).

[26] M. J. Abraham, T. Murtola, R. Schulz, S. Páll, J. C. Smith, B. Hess, and E. Lindahl, SoftwareX **1**, 19 (2015).

[27] W. L. Jorgensen, D. S. Maxwell, and J. Tirado-Rives, J. Am. Chem. Soc. **118**, 11225 (1996).

[28] L. A. Girifalco, J. Phys. Chem. **96**, 858 (1992).

[29] See Supplemental Material at [URL to be inserted] for a discussion on the rotational effect of gas molecules.

[30] D. Timpel, K. Scheerschmidt, and S. H. Garofalini, J. Non-cryst. Solids **221**, 187 (1997).

[31] F. Cleri and V. Rosato, Phys. Rev. B **48**, 22 (1993).

[32] D. Beeman, J. Comput. Phys. **20**, 130 (1976).

[33] W. Feller, *Introduction to Probability Theory and Its Applications* (Wiley, New York, 1972), 2 edn., Vol. 2.

[34] O. M. Wilson, M. R. Knecht, J. C. Garcia-Martinez, and R. M. Crooks, J. Am. Chem. Soc. **128**, 4510 (2006).

[35] J. Jiang, G. Oberdörster, A. Elder, R. Gelein, P. Mercer, and P. Biswas, Nanotoxicology **2**, 33 (2008).

[36] K. Suttiponparnit, J. Jiang, M. Sahu, S. Suvachittanont, T. Charinpanitkul, and P. Biswas, Nanoscale. Res. Lett. **6**, 27 (2011).

[37] W. Thomson, Proc. R. Soc. Edinb. **7**, 63 (1872).

[38] H. Asada, Jpn. J. Appl. Phys. **19**, 2055 (1980).

[39] N. Miyoshi, K. Osuka, I. Kinefuchi, S. Takagi, and Y. Matsumoto, J. Phys. Chem. A **118**, 4611 (2014).

[40] V. Y. Rudyak, S. L. Krasnolutskii, A. G. Nasibulin, and E. I. Kauppinen, in *Doklady Physics* (Springer, 2002), pp. 758.

[41] Y. Kuga, K. Okauchi, D. Takeda, Y. Ohira, and K. Ando, J. Nanopart. Res. **3**, 175 (2001).

[42] H. G. Scheibel and J. Porstendo, J. Aerosol Sci. **14**, 113 (1983).

[43] J. Fernández de la Mora, L. De Juan, K. Liedtke, and A. Schmidt-Ott, J. Aerosol Sci. **34**, 79 (2003).

[44] A. G. Nasibulin, E. I. Kauppinen, B. A. Thomson, and J. Fernández de la Mora, J. Nanopart. Res. **4**, 449 (2002).

[45] S. Ude and J. Fernández de la Mora, J. Aerosol Sci. **34**, 1245 (2003).

TABLE I. Summary of MD results for a silver particle in a bath of nitrogen.

R (nm)	N/N_0 [a]	T (K)	μ_{esc}	$-\Phi(r^*)$ (K)	$\bar{E}'$ (K)	λ	c	π MD	π Eq. (11)[b]	π Eq. (11)[c]
0.5	1	300	1.33	159	471	0.86	0.40	0.13	0.06	0.12
0.75	1	300	1.29	227	493	0.81	0.52	0.22	0.28	0.27
1	1	300	1.49	273	506	0.80	0.53	0.30	0.32	0.38
1.5	1	300	2.19	340	519	0.80	0.44	0.44	0.52	0.53
2	1	300	2.17	378	527	0.80	0.48	0.63	0.60	0.60
1	0.5	300	1.74	273	501	0.82	0.46	0.33	0.37	0.38
1	2	300	1.49	273	494	0.84	0.49	0.31	0.32	0.38
1	1	150	2.67	273	281	0.79	0.52	0.76	0.80	0.82
1	1	250	1.76	273	429	0.80	0.51	0.49	0.50	0.50
1	1	350	1.40	273	578	0.81	0.50	0.27	0.31	0.29
1	1	450	1.10	273	718	0.84	0.52	0.20	0.21	0.17
Average:			$\mu_{esc} = -1.45\Phi(r^*)/c\bar{E}'$			0.80±0.02	0.49±0.04			

[a] $N_0 = 2.45\times10^{19}$ cm^{-3}. [b] Evaluated using μ_{esc}, λ , and c values shown for each case. [c] Evaluated using the μ_{esc} expression and average λ, and c values shown in the bottom line of the current table.

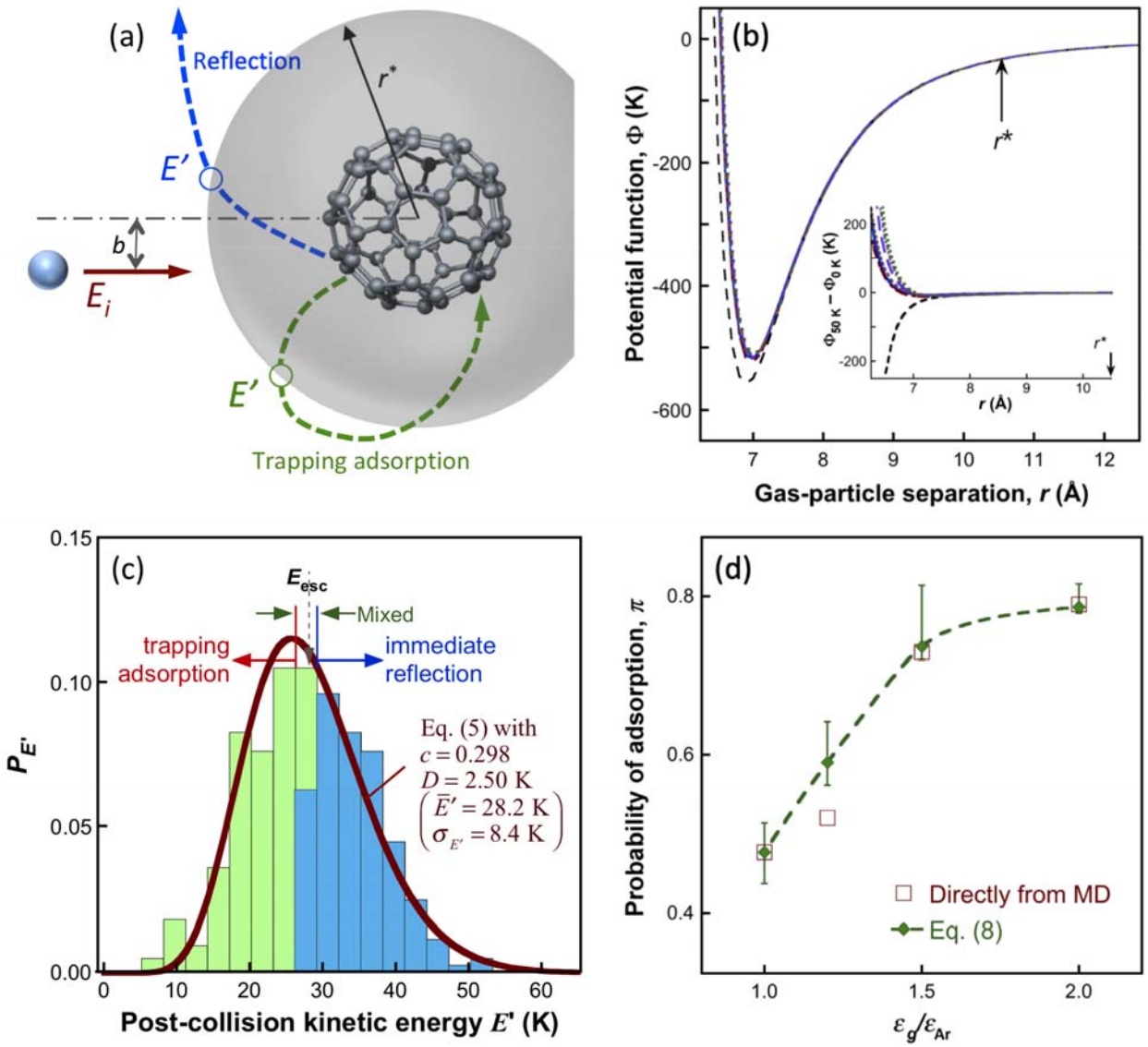

FIG. 1. Collision dynamics of C_{60} with Ar. (a) Illustration of two collision scenarios. (b) The Ar-C_{60} potential functions (r is measured from the C_{60} mass center) sampled from 10 MD trajectories at the C_{60} vibration temperature of 50 K, incident Ar velocity of 72.5 m/s, and the impact factor b = 0. Inset: the differences of the potential energy between 50 K and 0 K for C_{60}. (c) The E' distribution under the condition same as panel (b). Lighter (green) bars indicate surface adsorption; darker (blue) bars represent immediate reflections under the same condition as (b). Line: Gamma distribution fit. (d) The probability of surface adsorption over a range of well depth relative to that of Ar. The error bars illustrate the sensitivity of π to E_{esc} with the upper and lower bars representing 25% and 75% of the gas undergoing immediate reflections, respectively. The dashed line is drawn to guide the eyes.

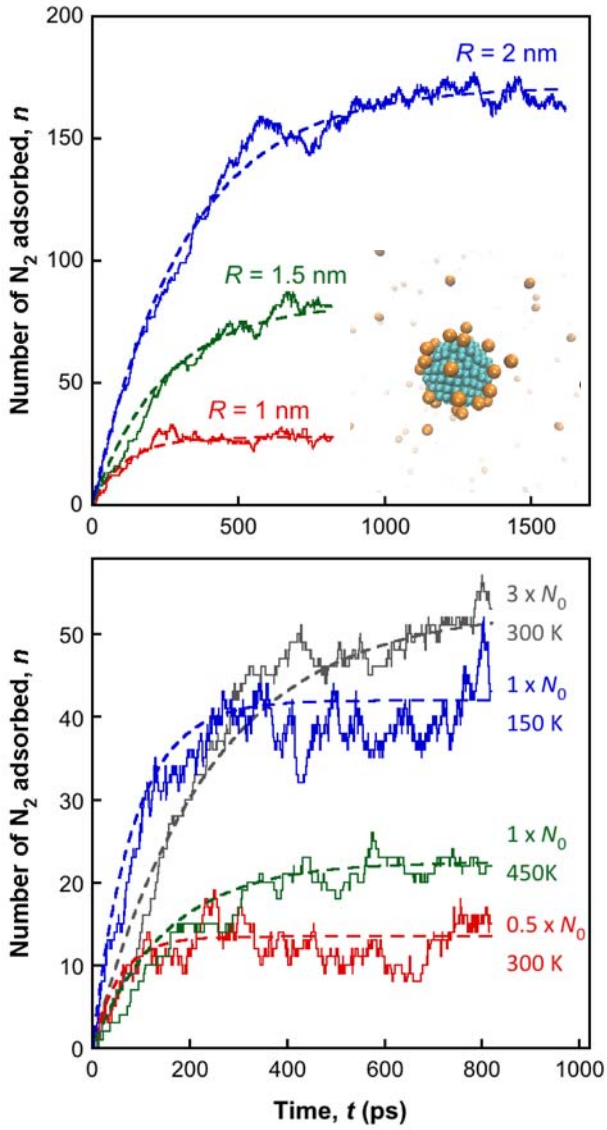

FIG. 2. Time evolution of the number of N_2 molecules absorbed on the Ag particle for several particle radii at $T = 300$ K and $p = 1$ atm (top panel) and at several combinations of temperature and gas number density for a fixed particle radius $R = 1$ nm. Solid lines: MD simulations; dash lines: fits to MD results using Eq. (10). Inset in the top panel: An MD snapshot of a silver particle ($R = 1$ nm) in 863 N_2 molecules ($T = 300$ K, $p = 1$ atm).

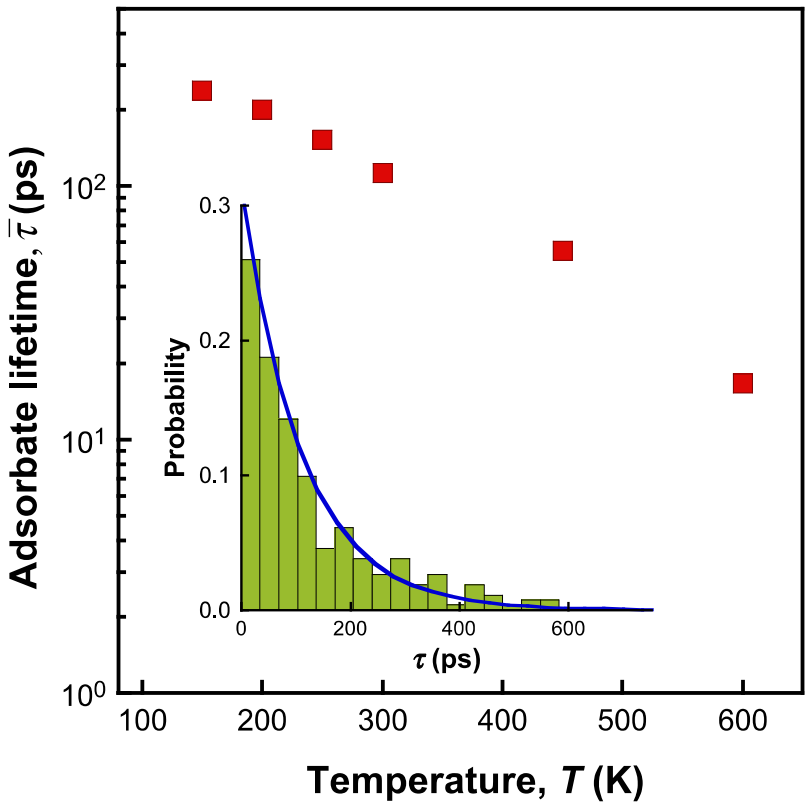

FIG. 3. Mean lifetime of the adsorbate N_2 on a Ag particle (R = 1 nm) as a function of temperature at 1 atm pressure. Inset: histogram of the lifetime of adsorbed N_2 under the same condition. The line is an exponential fit to the distribution.

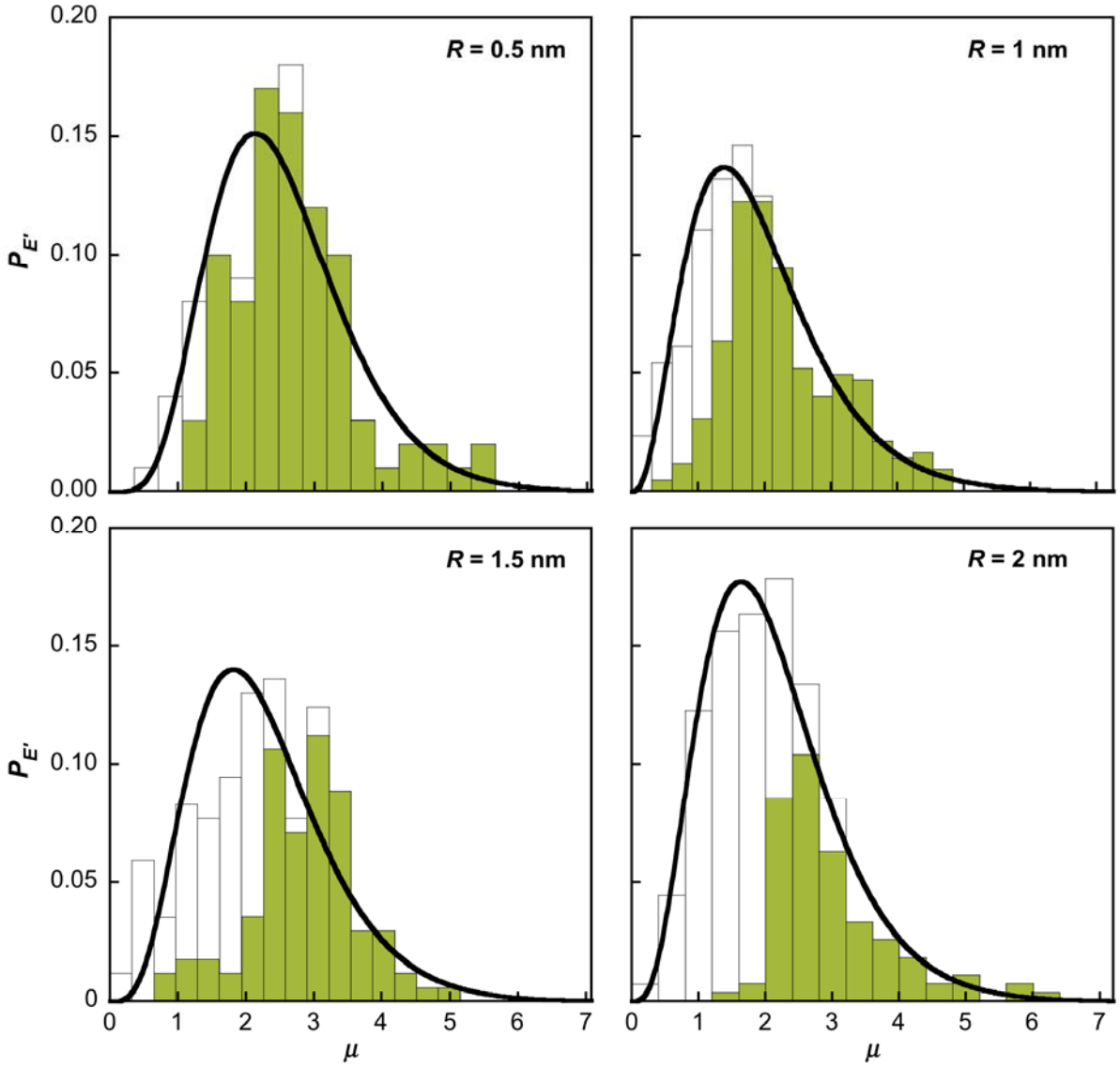

FIG. 4. Nondimensionalized post-collision energy distributions evaluated at $r^* = R + 0.5$ nm for four particle radii. Each distribution is obtained from evaluating >100 MD trajectories of collisions of N_2 with an Ag particle with the system temperature of 300 K and pressure of 1 atm. Lines: fits to the Gamma distribution function. The shaded histogram bars represent the immediate reflection events and the open bars represent surface adsorption.

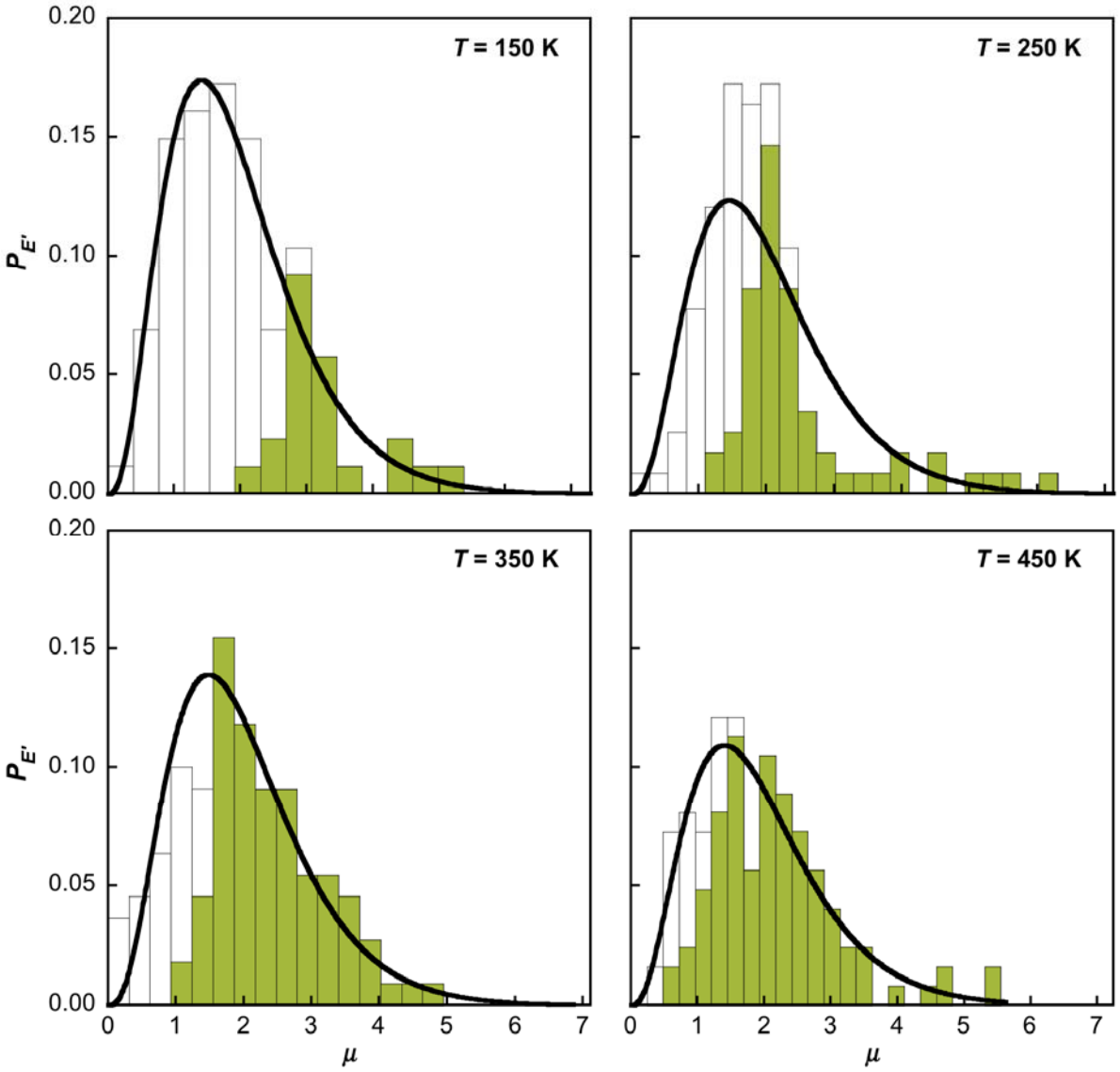

FIG. 5. Nondimensionalized post-collision energy distributions evaluated at $r^* = R + 0.5$ nm for N_2 collisions with an Ag particle with $R = 1$ nm evaluated at four system temperatures. Each distribution is obtained from evaluating >100 MD trajectories of collisions of N_2 at the pressure at 1 atm. Lines: fits to the Gamma distribution function. The shaded histogram bars represent the immediate reflection events and the open bars represent surface adsorption.

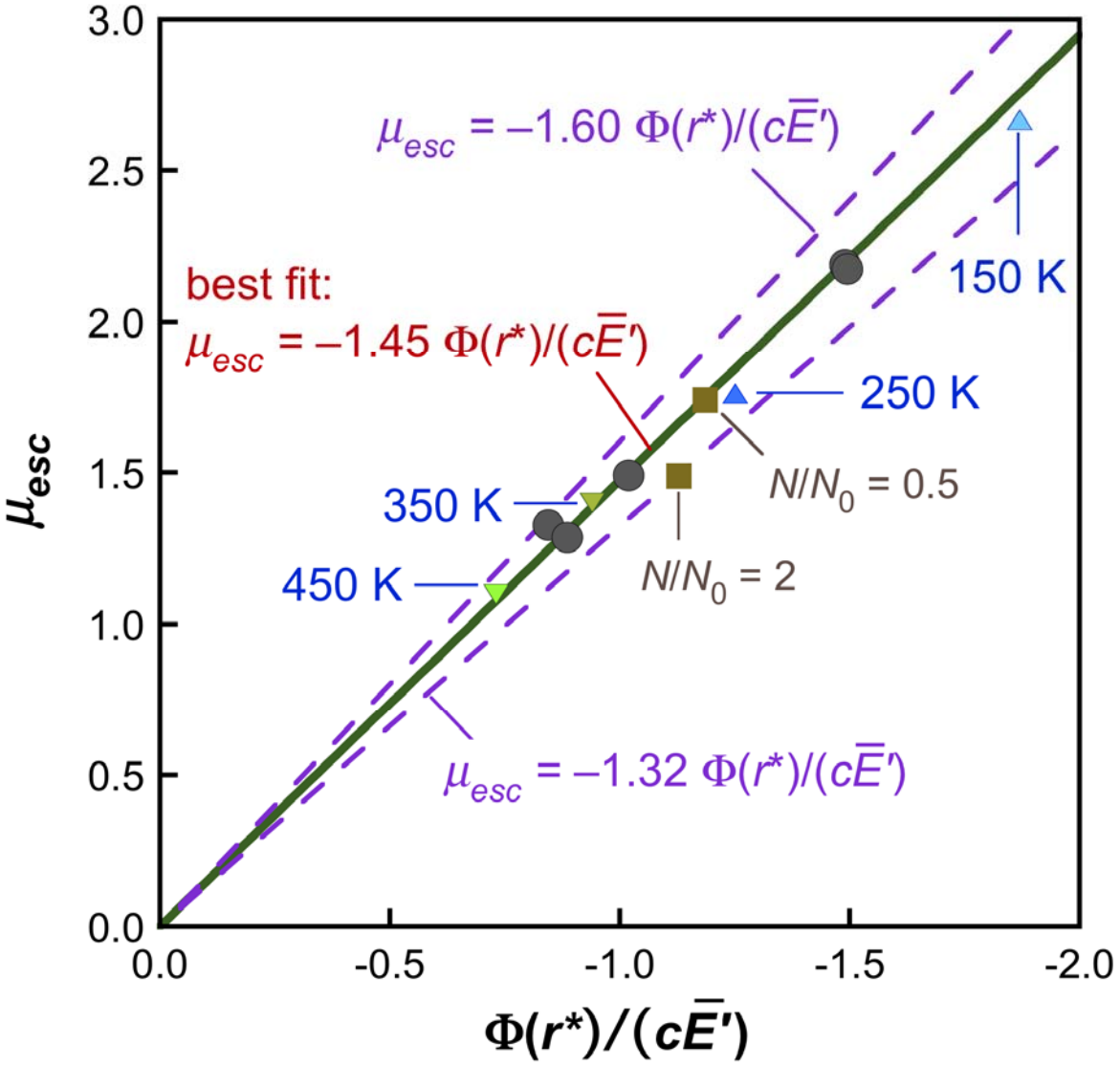

FIG. 6. Dimensionless escape energy of N_2 with silver particles determined from MD simulations of particle radii R = 0.5, 0.75, 1, 1.5, and 2 nm at 300 K and 1 atm is represented by the circle symbols as a function of dimensionless potential energy $\Phi\left(r^*\right)/c\bar{E}'$. The solid line is the fit to . The triangle symbols denote the MD results at 150, 250, 350 and 450 K as shown. The squares represent results at 300 K but with different gas densities (pressures). The dashed lines bracket the uncertainty in the coefficient.

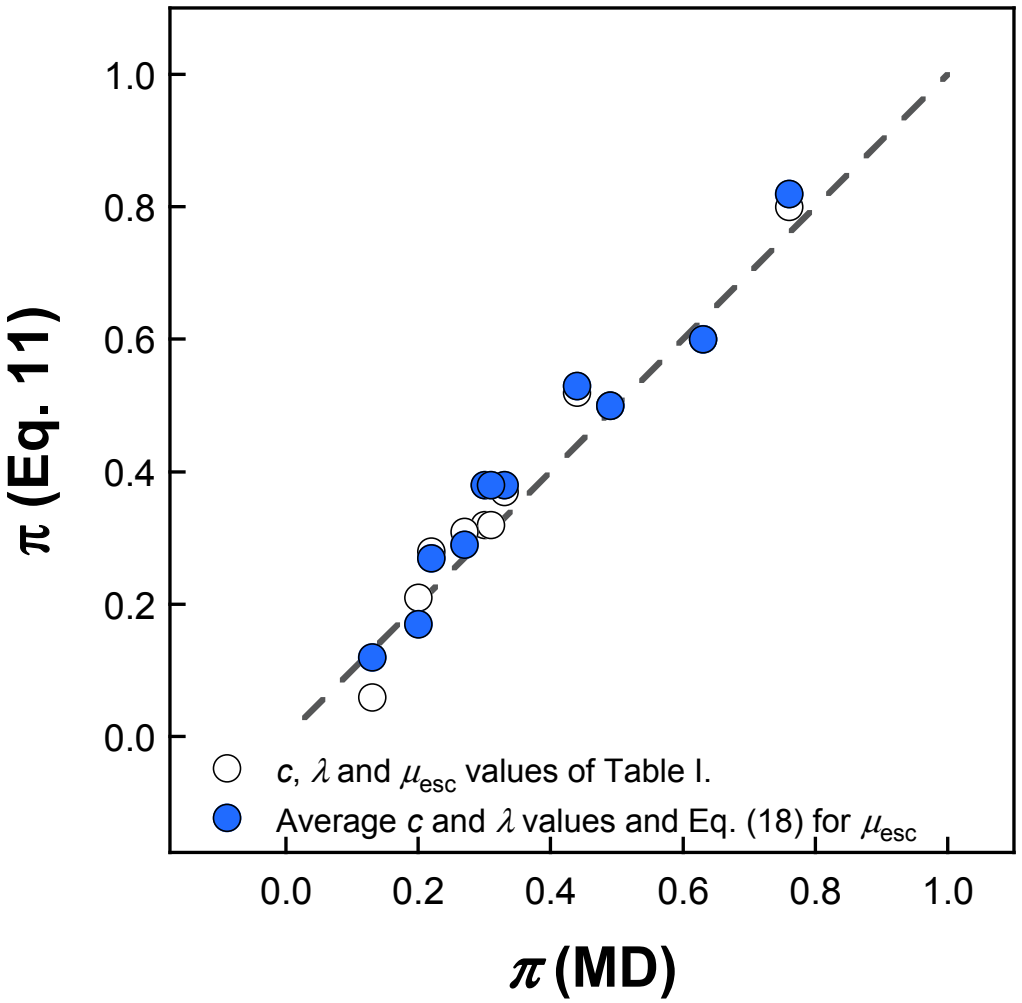

FIG. 7. Comparison of the probabilities of surface adsorption by Eq. (11) and those directly evaluated with MD over the conditions listed in Table 1.

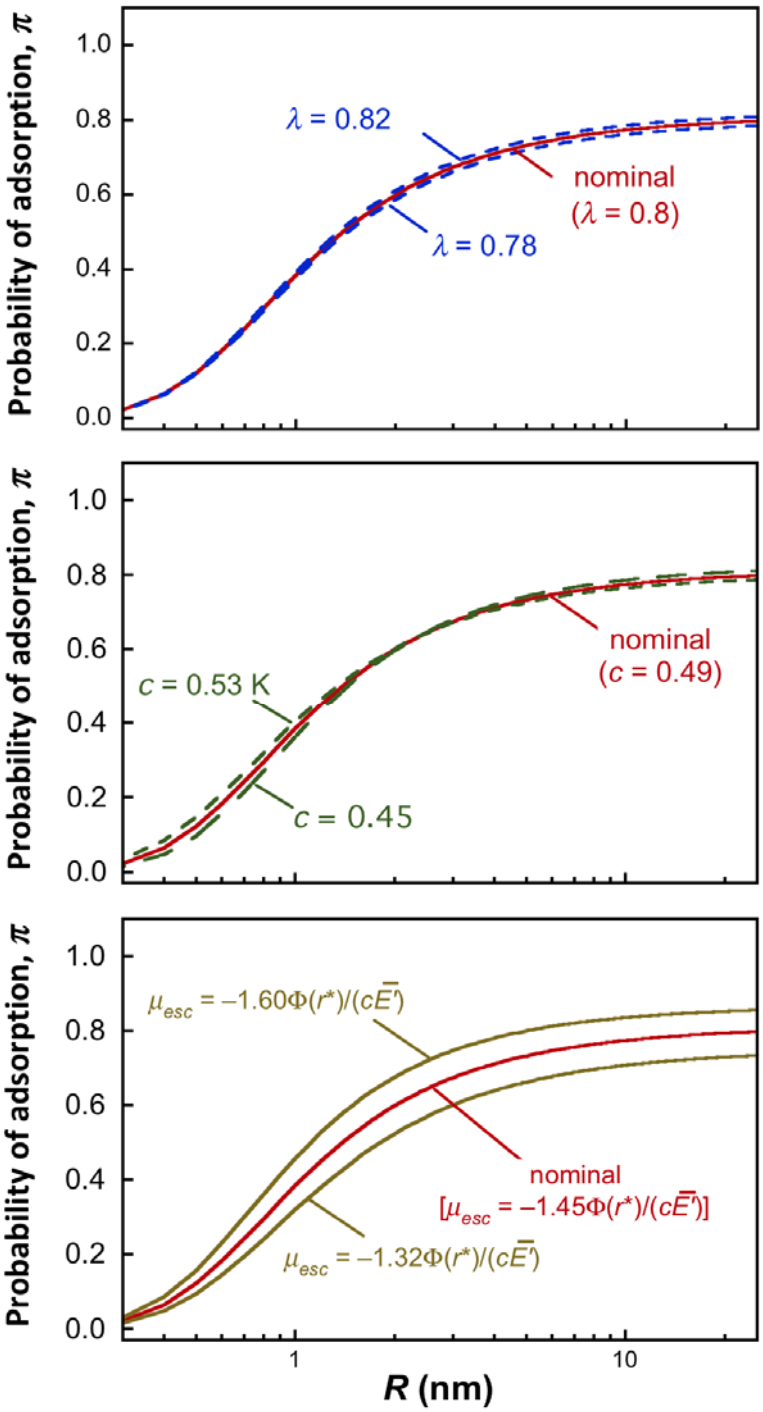

FIG. 8. Sensitivities of surface adsorption probability π with respect to the energy accommodation factor λ (a), the coefficient of dispersion c (b), and the dimensionless escape energy μ_{esc} (c), all at 300 K for an Ag particle in an N_2 bath.

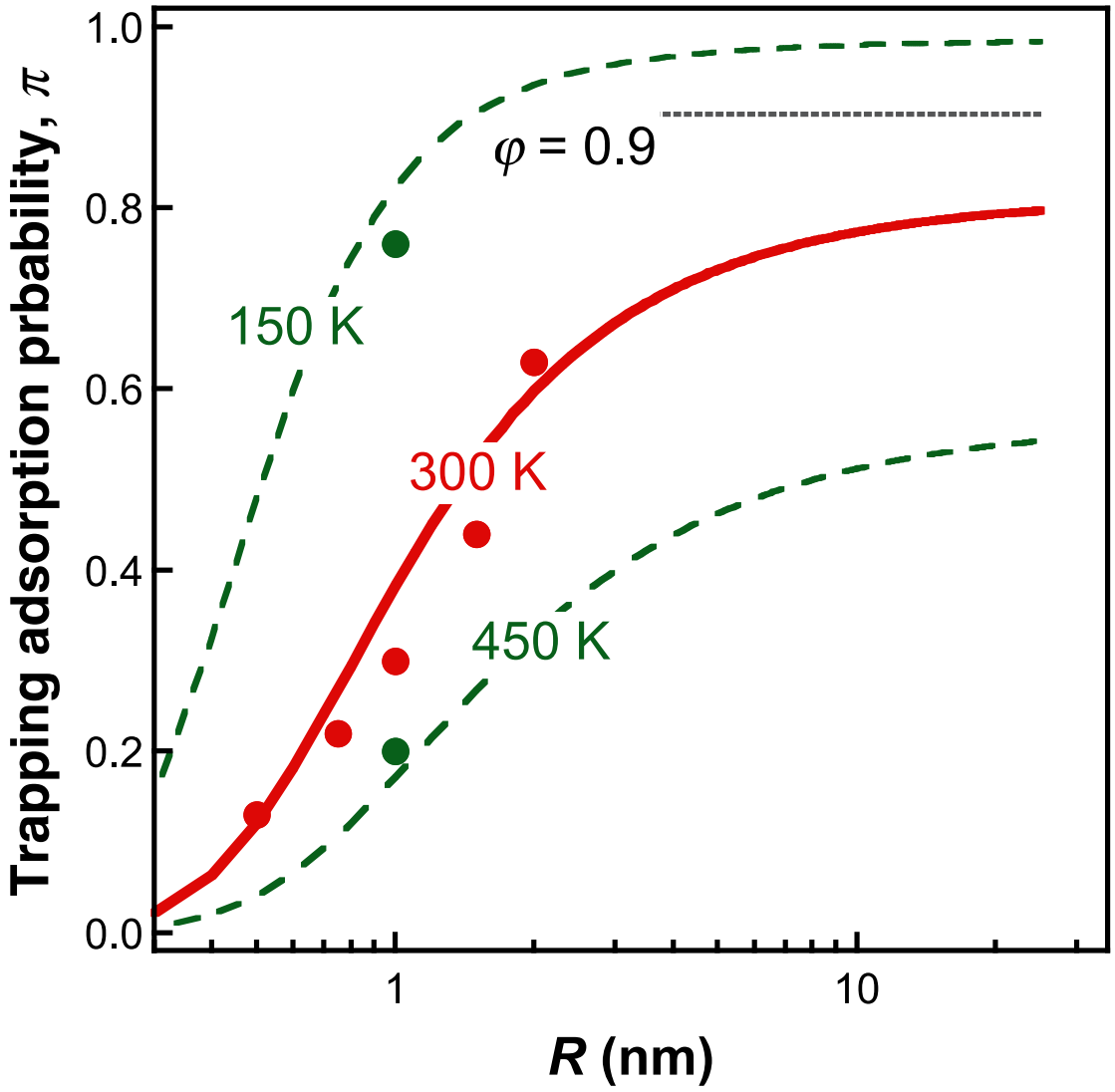

FIG. 9. Probability of adsorption or equivalently, momentum accommodation coefficient of silver particle in N_2 as a function of particle radius R at the indicated temperature and 1 atm pressure. The lines are the predictions of Eq. (11); the symbols are from MD simulations (see, Table 1).

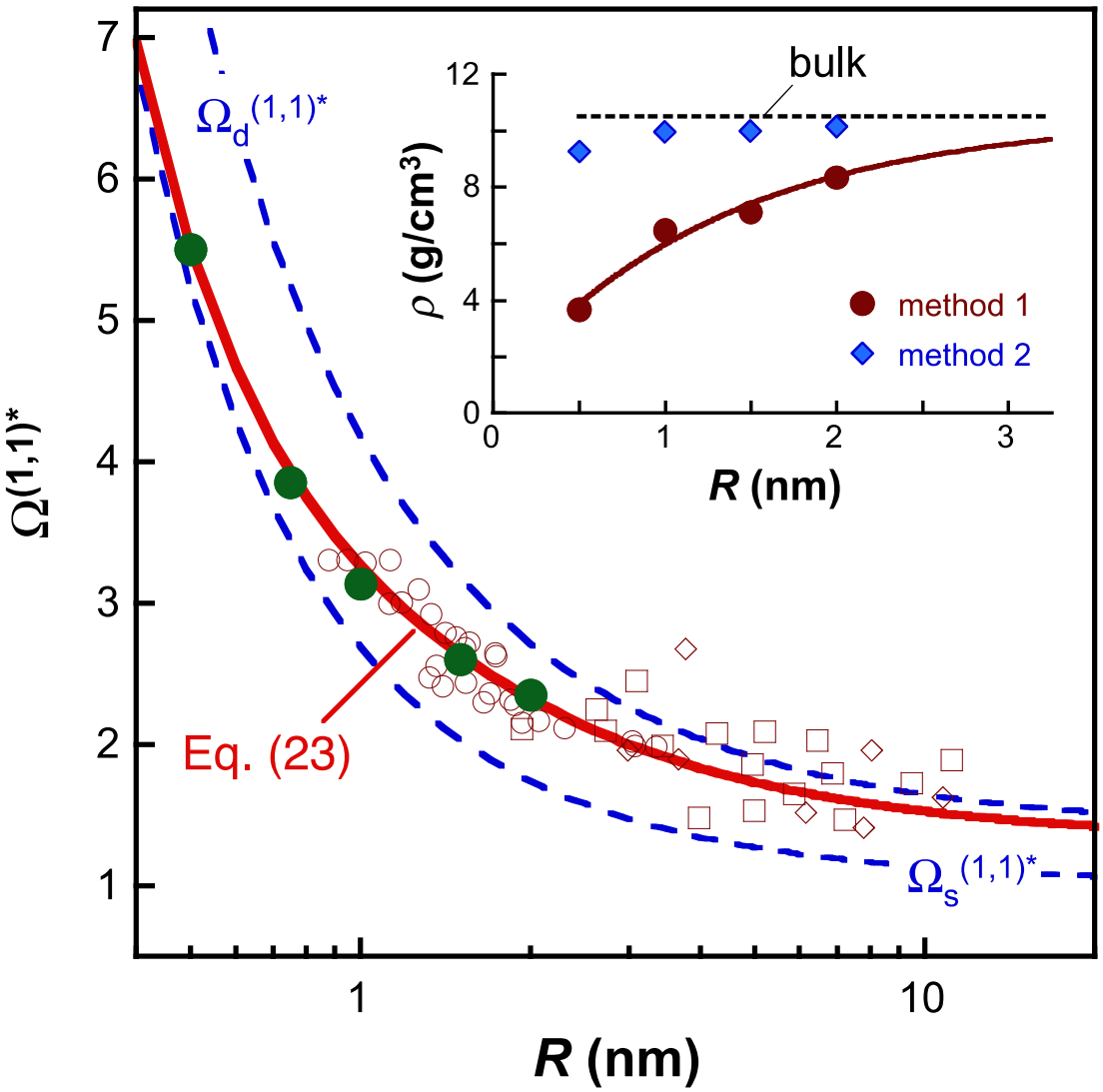

FIG. 10. The reduced collision integral in the specular and diffuse collision limits (dashed lines) and the experimentally-derived collision integral values (diamonds: [41], squares: [42], open circles [43]). The solid line is the prediction (Eq. 23); solid symbols: from MD directly using $\Omega^{(1,1)*} = \varphi\Omega_s^{(1,1)*} + (1-\varphi)\Omega_d^{(1,1)*}$. Inset: material density of Ag from MD using two methods (see text).

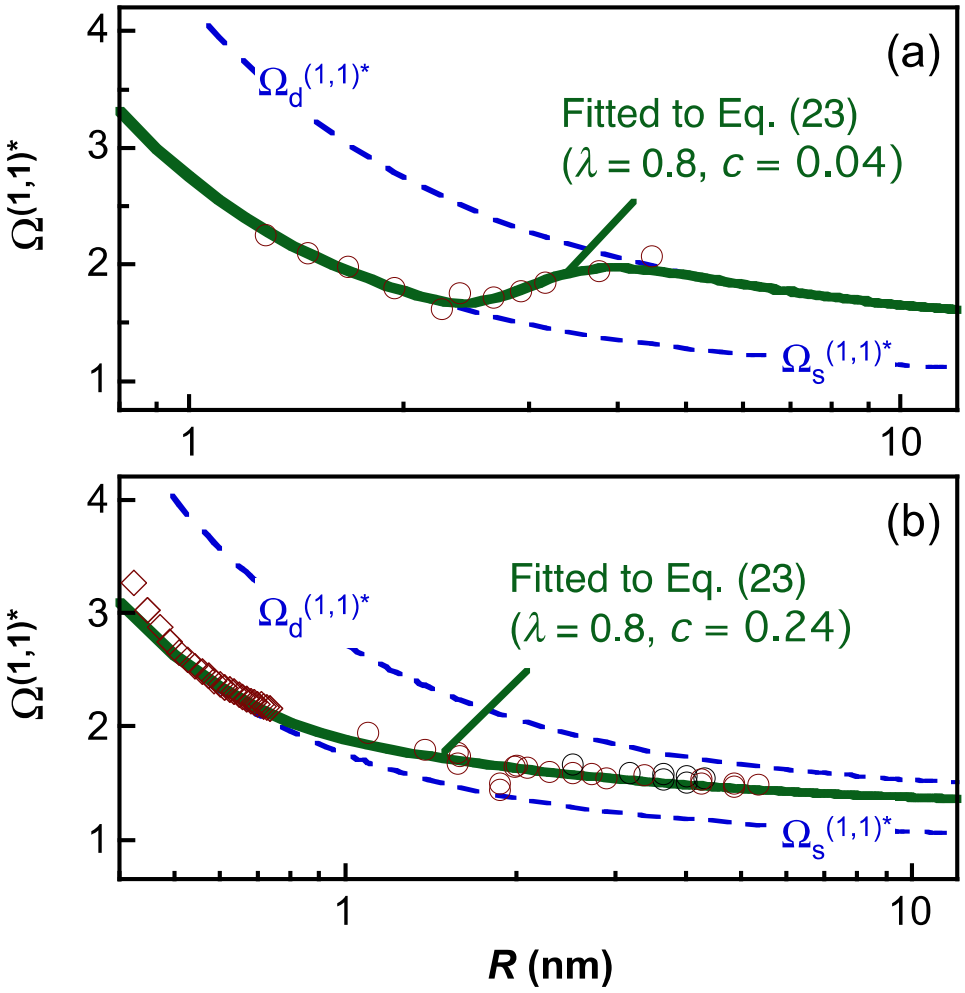

FIG. 11. The experimentally-derived (symbols), fitted using Eq. 23 (solid lines) and limiting reduced collision integral (a. Cu_2O [40], b. PEG: diamonds [40]; circles: [45]) as a function of the particle radius R.